PERGAMON

International Journal of Heat and Mass Transfer 45 (2002) 1117–1125

International Journal of HEAT and MASS TRANSFER

www.elsevier.com/locate/ijhmt

Pool boiling heat transfer and simplified one-dimensional model for prediction on coated porous surfaces with vapor channels

Wei Wu, Jian-Hua Du, Xue-Jiao Hu, Bu-Xuan Wang *

Thermal Engineering Department, Tsinghua University, Beijing 100084, China

Received 7 March 2001

Abstract

Boiling heat transfer on porous coated surfaces with vapor channels was investigated experimentally to determine the effects of the size and density of the vapor channels on the boiling heat transfer. Observations showed that bubbles escaping from the channels enhanced the heat transfer. Three regimes were identified: liquid flooding, bubbles in the channel, and dry-out. The heat transfer coefficient and $\dot{q}_{cr}$ of the porous surfaces with vapor channels were much higher than those on the smooth surface. The maximum heat transfer occurred for an optimum vapor channel density and the boiling heat transfer performance was improved if the channels were open. According to observations, vapor could escape through the vapor channel while liquid was sucked by a porous structure, and hence, the two-phase region will extend to a pool liquid at a given flux. This indicates that capillarity plays a great effect on the boiling and the heat transfer performance can be increased significantly. A simplified one-dimensional formulation for the two-phase flow within such a heterogenous structure was proposed using an equivalent dual porous model. It is demonstrated theoretically that the geometric dimensions and the density of vapor channels affect the boiling heat transfer. This may provide a new key for enhancing boiling heat transfer by capillary porous structure.

Keywords: Pool boiling; Porous surface; Vapor channels

1. Introduction

The enhanced boiling heat transfer on porous surfaces has been of considerable research interest due to its effectiveness and numerous applications such as in boilers, heat pipes and for the cooling of micro-electronic components. The porous layers can be manufactured by various methods such as machining, welding, sintering or brazing of particles, electrolytic deposition, flame spraying, bonding of particles by plating, galvanizing, plasma spraying of polymers, metallic coating with foam substrates, etc. Boiling heat transfer on surfaces with isotropic capillary coatings has been studied for different specific applications since the 1970s [1]. The transport phenomenon is affected by many factors such as the working fluids, skeleton material, shape and the dimensions of the micro-structure, saturate condition and so on. Some systematic experimental studies have been made to understand the boiling and two-phase flow mechanism. The effects of isotropic coating parameters such as porosity, permeability, thermal conductivity and thickness on heat transfer have been examined [2]. The enhanced boiling heat transfer on porous coated surfaces may be attributed to the numerous potential nucleation sites, the continuous evaporation inside the pore structure, the bubble ejection from the top surface of the layer and liquid suction from the pool.

* Corresponding author. Tel.: +86-10-6278-4530; fax: +86-10-6277-0209.

E-mail address: bxwang@mail.tsinghua.edu.cn (B.-X. Wang).

0017-9310/02/$ - see front matter
PII: S0017-9310(01)00192-2

Nomenclature

A_ℓ	liquid cross-sectional area of wicks (m^2)
A_v	vapor occupied area (m^2)
CAR	channel area ratio (%)
D_C	vapor channel hydraulic diameter (m)
f	friction factor (non-dimensional)
$h_{\ell v}$	special enthalpy (J/kg)
H	height of wicks (m)
$J(S)$	Levertt function (non-dimensional)
K	permeability (m^2)
m	evaporation mass flux (kg/m^2 s)
N_C	the number of opened channels ($1/m^2$)
$\dot{q}_{cr}$	dry-out heat flux (W/m^2)
S	saturation (non-dimensional)
W	channel width (m)

Subscripts

c	channels
e	evaporate or equivalent
ℓ	liquid
p	particle
v	vapor
0	value of $z = 0$

Greek symbols

μ	dynamic viscosity (Pa s)
σ	surface tension (N/m)
ϕ	volume porosity (non-dimensional)
v	kinematics viscosity (m^2/s)
ρ	density (kg/m^3)

Thin porous coating can promote nucleation, and hence, intensify the heat transfer at low heat flux. However, the high flow resistance of the porous media to the vapor will promote the formation of a vapor layer near the heated surface so as to cause transition from nucleate to film boiling.

The idea for vapor channels on the porous coating has been motivated by the experiments of Moss and Kelley [3], from which vapor produced on the heated surface flowed along the base of the wick at first and then escaped through the larger pore path. It can be expected that the boiling heat transfer coefficient and the critical heat flux can be increased by porous surface structures with vapor channels to facilitate the vapor outflow. Malyshenko [4] initially experimentally investigated the effect of vapor channels in the porous coating on the boiling curve. Plumb [5] examined the effects of the vapor channel density on the heat transfer in the background of evaporation in heat pipes. Their experimental results showed that boiling heat transfer coefficient can improve 3–2 times with 10–20% area ratio vapor channels. Recently, Stubos and Buchlin [6] analyzed the effect of vapor channels on boiling in a porous surface. Further experiments need to check existing models and to optimize the configurations for various conditions [7].

In this paper, we report our experimental results for pool boiling heat transfer of R11 on surfaces with various vapor channel configurations. The object is to examine the effects of channel size and density. The results demonstrate that vapor escapes from the open channels in which the liquid is sucked into the porous structure by a capillarity effect to enhance the heat transfer performance at high heat flux. The results make sure that there exists an optimal channel configuration to optimize the boiling heat transfer characteristics on porous coating surfaces with vapor channels. A simplified one-dimensional model is proposed for prediction.

2. Experiment

The pool boiling test facility used for the present work is shown in Fig. 1. A stainless steel container with glass windows, 225 mm high and 154 mm in diameter, was used for the boiling liquid pool containing about 150 mm high saturated R11 at atmospheric pressure. Heat flux was applied to the boiling surface through a copper column from an electric heater controlled by an AC voltage regulator. Heat transfer rate was calculated

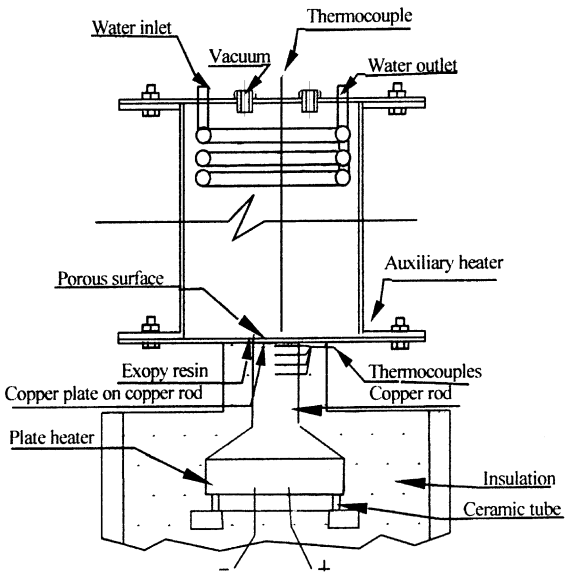

Fig. 1. Experimental setup.

from temperature gradient along the column, which was measured by three sets of Teflon coated copper–constantan (Omega) thermocouples. A HP-34970A data acquisition system was used with a digital voltmeter having a sensitivity of ±1 μV, a six-figure scale and an accuracy of 0.01% of the reading. The temperature measurement precision was calibrated previously to be within 0.2 °C and the thermocouple positions are precisely located within ±10 μm. The relative error of the heat flux was estimated to be within 4.2%. A cooling loop in the container controlled the liquid saturation temperature. The saturation condition was monitored with a U-type mercury manometer and was maintained by an auxiliary heater that was connected to an AC regulator.

The porous media was made from a bronze powder (Cu89%Sn8%Pb3%) and screened, using three mesh sizes −40 to +60, −100 to +120 and −180 to +200, respectively. The mean particle diameters are given in Table 1. The porous media permeability was provided by the manufacturer, which was measured by gas N_2. The porosity was 0.38, which was measured by filling the porous media sample with melted wax and verified through weighing samples and measuring their volume. The heated plate was first electroplated by 2–3 μm nickel in an oxygen-free oven at 860–920 °C, and then, the porous media was sintered to the surface. The vapor channels were produced by module simultaneously, with channel configurations listed in Table 1. In addition, two layer structures were tested too. The tested surface was 30 mm wide, 30 mm long, and about 7 mm thick, as shown in Fig. 2.

The surfaces of the test plate and the copper column were polished with 500 mesh diamond abrasives and glued with thermal glue to make their contact as good as possible. Nine thermocouples were embedded in the test plate, 1 mm below the boiling surface. The temperature on the boiling surface was then calculated by Fourier's law. The test surface was positioned at the bottom of the container with epoxy resin. The test vessel was insulated with 15 mm thick elastic foam insulation.

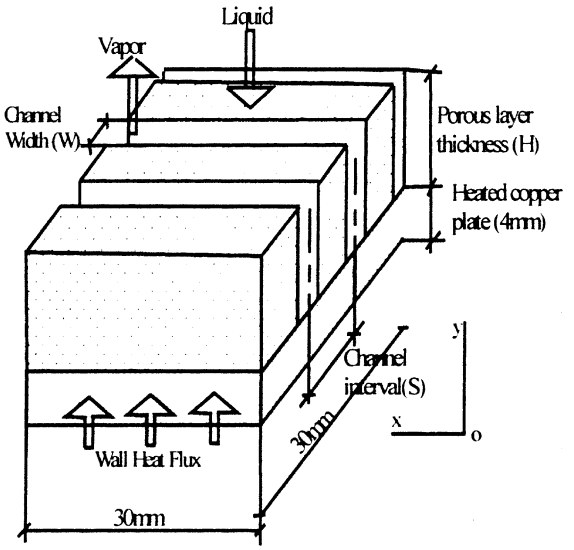

Fig. 2. Test surface structure (unit: mm).

After installation, the container was evacuated and filled with the working fluid R11. Before the experiments, the test surface was soaked and cleaned with acetone to remove any oil. Uncondensable gases were removed during the experiments if the vapor pressure was higher than the saturation pressure corresponding to the liquid temperature in the pool. The unit was heated in a way for heat flux decreasing stepwise in order to avoid the effects of boiling hysteresis. The heating

Table 1
Test surfaces

Mean particle size (μm)	Permeability $\times 10^{-11}$ (m^2)	Porous layer thickness (H) (mm)	Number of channels	Channel width (W) (mm)	Channel separation (S) (mm)	Channel depth (H) (mm)	Channel area ratio (CAR) (%)
250	4.5	3	0	–	–	–	0
250	4.5	3	5	0.8	4.3	3	13
250	4.5	3	6	0.8	5.0	3	16
250	4.5	3	8	0.8	6.0	3	21
110	0.9	2.6	0	–	–	–	0
110	0.9	2.6	9	0.67	3.07	2.6	20
110	0.9	2.6	8	1.05	3.45	2.6	28
110	0.9	2.6	7	1.54	3.94	2.6	36
110	0.9	2.6	6	2.20	4.60	2.6	42
65	0.03	2.4	0	–	–	–	0
65	0.03	2.4	9	0.78	3.08	2.4	23
65	0.03	2.4	8	1.16	3.46	2.4	31
65	0.03	2.4	7	1.66	3.96	2.4	38
65	0.03	2.4	6	2.32	4.62	2.4	46

power went up to the highest at first and dropped stepwise per measurement to the lowest. It took about 10–30 min for the steady state to be attained and the measurement could be made thereby. The heat flux value calculated from heating power equaled what was measured by the thermocouple matrix on the steel block approximately. Measurements were made until steady boiling state was attained at each setting. The boiling conditions were also recorded. Heat flux was increased in a stepwise about intervals of 2.0 W/cm^2.

Measuring the boiling heat transfer on a smooth copper surface checked the reliability of the experimental apparatus first. The heat flux as a function of the wall superheats, compared with Rohsenow's correlation [1] in Fig. 3, showed that the experimental results would be reliable.

Three regions can be roughly examined from the attached experimental photos: liquid flooding, bubbles in the channel, and dry-out. For boiling on the various porous coatings, at superheats approximately 1 °C, bubbles occurred on a few spots of the porous coating surface at bottom intersection with channel's smooth surface. The wall superheats of temperature overshoot were less than 3 °C, due to uneven temperature distribution between the porous coating surface bottom intersection with channel's smooth surface. The heat transfer coefficient of porous surfaces was much higher than that of the smooth surface. The boiling hysteresis on porous surfaces with vapor channels is not obvious. The widely separated bubbles had a great influence on the heat transfer. With increasing wall superheats above 3 °C, the heating surface became populated with bubbles. The heat transfer coefficient on the porous surfaces was two to ten times greater than that on the smooth surface with corresponding superheats increased from 3 to 30 °C, due to the active bubble formation and frequent bubble departure within the porous structure with vapor channels in the porous surface. The vapor escaped from the channels, while the liquid was sucked into the heated surface by the capillarity force of the porous structure. This ordered vapor–liquid flow improved further the boiling heat transfer on the porous coated surfaces. Then, the vapor produced in certain pores, which are called vapor pores, went outside from the channel. A very thin film was held in the skeleton of the porous coating forming liquid meniscuses. Liquid in these meniscuses evaporated continually, making the bubbles on the active pores grow up and departed in a very short period through the vapor pores.

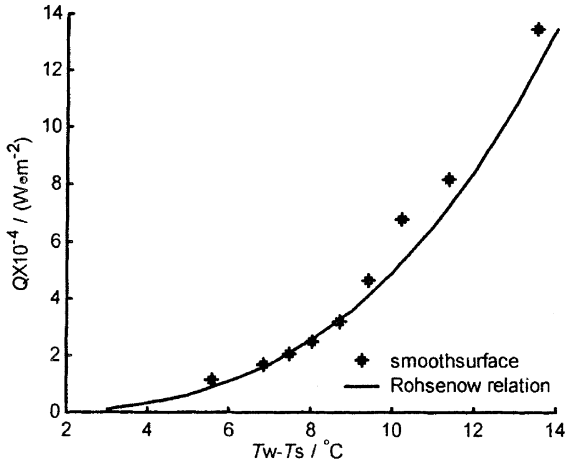

Fig. 3. Heat flux for R11 boiling on a smooth copper surface.

When bubbles are expanding out to channel, the pressure inside porous coating is going down, which makes the liquid in the outer pool to be sucked in the channel through inactive pores by capillarity force. The sucked liquid flowed along the skeleton of the porous coating to supply the liquid that had evaporated. This process is driven by the capillarity force produced by liquid–vapor surface tension. The intensive evaporation not only augmented the evaporation heat transfer itself, but also augmented the convective heat transfer effect. This operating region may be called Suction–Evaporation Cycle Mode. At still lower superheat, most of the tunnel space is occupied by the liquid, and an active pore operates like an isolated nucleation site at a few spots of the porous coating surface bottom section with channel smooth surface. This is the Flooded Mode. At larger superheat, about 30 °C in this work (which was different with various porous coating thicknesses and CAR), the thermocouple temperature difference is larger than 20 °C, which indicates a dry-out spot on the boiling surface. Therefore, the nine-thermocouple readings were averaged to determine the surface temperatures during the tests. According to the literature [10], $\dot{q}_{cr}$ was assumed and we recorded the value to compare the improvement of $\dot{q}_{cr}$. For superheats from 30 to 45 °C, the evaporation rate was so high that vapor bubbles emerged from the porous coating surface, as well as from the vapor channels. The temperature difference still increased slowly until porous surfaces operated like a smooth surface ultimately when the increased number of active sites and pressure inside the skeleton of the porous coating prevented liquid from entering through pores into the heated surface, which occurred at superheat much higher than 45 °C. This is not discussed in this work.

The experimental results are summarized in Figs. 4–6. It can be seen from Fig. 4 that, for the #110 porous surface, the heat transfer rate on the surface with eight vapor channels was the highest. For the #250 porous surface in Fig. 5, the heat transfer rate on the surface with six vapor channels was higher than either the surface with eight channels or that with five channels, suggesting an optimum configura-

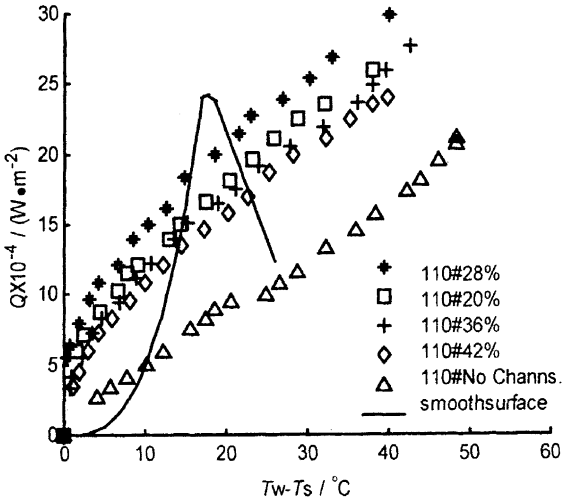

Fig. 4. Heat flux for R11 boiling on the #110 surfaces.

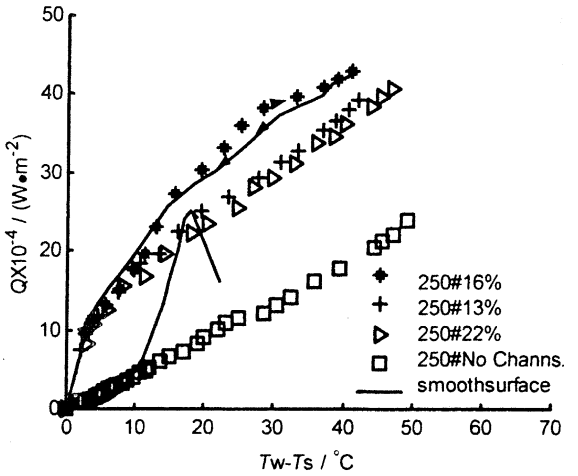

Fig. 5. Heat flux for R11 boiling on the #250 surfaces.

tion of vapor channels. In Fig. 6, the boiling heat transfer rate on #65 surface with seven vapor channels was the highest.

The results also showed that the vapor channels on the porous surface may affect the boiling hysteresis. The experimental results for the #250 surface with six vapor channels are plotted in Fig. 5 as the heat flux was increased (the symbols) and decreased (the arrows). From our experiment, the boiling hysteresis on porous surfaces is much less that that on smooth surfaces, but too many channels (more than optimal number of channels) will aggravate the hysteresis of boiling.

The $\dot{q}_{cr}$ of porous surfaces with vapor channels was about 2–4 times than that for isotropic porous surface in Figs. 4–6 and the dry-out heat flux was about 3.5×10^5, 2×10^5 and 1.0×10^5 W/(m^2 K) for 250, 110 and 65 μm,

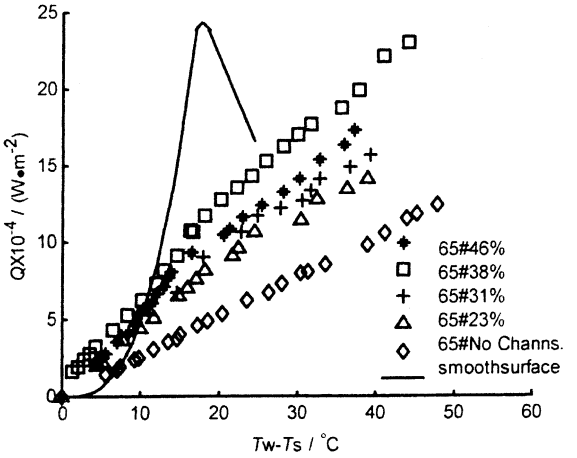

Fig. 6. Heat flux for R11 boiling on the #65 surfaces.

respectively. The $\dot{q}_{cr}$ of #250 porous surfaces was about 1.5 times than that on the smooth surface. The $\dot{q}_{cr}$ for smooth surface was obtained from Zuber's formula [1].

3. Model development

In this work, we try to investigate theoretically the fluid flow and heat transfer in porous coatings with open channels. A simplified one-dimensional model was proposed based on our dual porosity model [9], in which the pressure difference between liquid and vapor was balanced by capillary force. The fully thermal contact between coating and heated surface was assumed and resistance to vapor flow in the channels was taken into consideration. The effect of channel dimension on vapor flow and heat transfer was also examined, and an optional density of area vented for vapor on porous surface can be predicted thereby.

Fig. 7 illustrates the configuration of venting porous wicks. It is assumed that representative element of volume consists of two different transport porous media: P (porous) and C (channel) the volumes of which are V_P and V_C, respectively. Their porosity, permeability and relative permeability are represented by ϕ_j, $k_{ri,j}$ ($i = \ell, v$) and K_j ($j = P, C$), respectively.

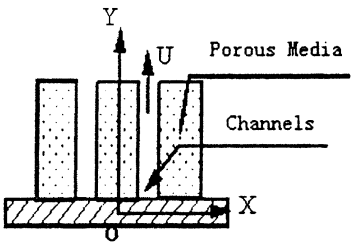

Fig. 7. Analytical model.

Obviously, $V = V_P + V_C$, and so, the averaged porosity will be

$$\phi = \frac{\phi_P V_P + \phi_C V_C}{V} = \phi_P \frac{V_P}{V} + \phi_C \frac{V_C}{V},$$
where $\phi_C = 1$. (1)

The liquid saturation in the representative element of volume is

$$S = \frac{\phi_P V_P S_P + \phi_C V_C S_C}{\phi_P V_P + \phi_C V_C}. \quad (2)$$

It is assumed that the flow of the vapor and liquid in P and C is one-dimensional Darcy flow along the direction normal to the heated transfer. Therefore

$$\dot{m}_{i,P} = -K_P k_{ri,P}\left(\frac{\rho_i}{\mu_i}\right)\left(\frac{dp_{i,P}}{dx} - \rho_i g\right), \quad (3a)$$

$$\dot{m}_{i,C} = -K_C k_{ri,C}\left(\frac{\rho_i}{\mu_i}\right)\left(\frac{dp_{i,C}}{dx} - \rho_i g\right), \quad (3b)$$

where the subscripts $i = \ell, v$ represent the liquid and vapor, respectively. If further assuming that pressure of liquid and vapor are equal in P and C, that is, $\nabla p_{i,P} = \nabla p_{i,C}$, the mass flow of liquid and vapor in the porous media can be written as follows:

$$\dot{m}_i = \dot{m}_{i,P} + \dot{m}_{i,C} = -(K_P k_{ri,P} + K_C k_{ri,C})\left(\frac{\rho_i}{\mu_i}\right)\left(\frac{dp_i}{dx} - \rho_i g\right). \quad (4)$$

Hence, the heterogenous porous media can be treated as an equivalent homogenous media of which the effective permeability will be [11]

$$K = \frac{\phi^3 D^2}{180(1-\phi)^2}, \quad D = \frac{D_P}{V_P}(V_P + V_C).$$

The equivalent relative permeability is

$$k_{ri} = \frac{K_P k_{ri,P} + K_C k_{ri,C}}{K}. \quad (5)$$

The mass flow rates of liquid and vapor in the whole porous media can be represented, respectively, as

$$\dot{m}_\ell = -K k_{ri}\left(\frac{\rho_\ell}{\mu_\ell}\right)\left(\frac{dp_\ell}{dx} - \rho_\ell g\right), \quad (6a)$$

$$\dot{m}_v = -K k_{rv}\left(\frac{\rho_v}{\mu_v}\right)\left(\frac{dp_v}{dx} - \rho_v g\right). \quad (6b)$$

From the one-dimensional mass and energy conversation equation for steady boiling [11]:

$$\dot{m}_\ell + \dot{m}_v = 0, \quad (7)$$

$$q = \dot{m}_v h_{fg}. \quad (8)$$

The pressure gradients of liquid and vapor can be obtained from Eqs. (7), (8) and substitute into Eqs. (6a), (6b) as

$$\frac{dp_v}{dx} = -\frac{q v_v}{h_{fg} K k_{rv}} + \rho_v g, \quad (9a)$$

$$\frac{dp_\ell}{dx} = -\frac{q v_\ell}{h_{fg} K k_{r\ell}} + \rho_\ell g, \quad (9b)$$

where q is the heat flux at the wall and h_{fg} is the latent heat of vaporization of liquid. The capillary pressure gradient can be represented as: $p_C = p_v - p_\ell$:

$$\frac{dp_C}{dx} = -\frac{q}{h_{fg} K}\left(\frac{v_v}{k_{rv}} + \frac{v_\ell}{k_{r\ell}}\right) + (\rho_v - \rho_\ell)g. \quad (10)$$

The liquid distribution among P and C must satisfy the following condition:

$$p_C = p_v - p_\ell = \frac{\sigma}{\sqrt{K_P/\phi_P}} J(S_P) \quad (11)$$

in which $J(S_P)$ is the Levertt function which can be represented as [6]

$$J(S_P) = \frac{\left(S_P^{-1} - 1\right)^{0.175}}{\sqrt{5}}. \quad (12)$$

We can obtain from Eq. (11) that

$$\frac{dp_C}{dS} = \frac{dp_C}{dS_P}\frac{dS_P}{dS} = \frac{\sigma}{\sqrt{K_P/\phi_P}} J' \Big/ \left\{\frac{\phi_P V_P}{\phi_P V_P + \phi_C V_C}\right\}. \quad (13)$$

Combining Eqs. (10) and (13), we have

$$dx = \left[\left\{\frac{\sigma}{\sqrt{K_P/\phi_P}}\frac{f'}{\frac{\phi_P V_P}{\phi_P V_P + \phi_C V_C}}\right\} \Big/ \left\{-\frac{q}{h_{fg} K}\left(\frac{V_v}{k_{rv}} + \frac{V_\ell}{k_{r\ell}}\right) + (\rho_v - \rho_\ell)g\right\}\right] dS. \quad (14)$$

Substituting $k_{r\ell} = S^3$ and $k_{rv} = (1-S)^2$ in Eq. (14), provided that porous media parameter ϕ_j, k_{ri} $(i = \ell, v)$, K_j $(j = P, C)$ and V_P and V_C are known, the two-phase zone length in the equivalent porous media could be defined thereby [11].

The permeability of the channels can be deduced from the pressure drop formula for channels, i.e.

$$\Delta P_v = f_v \frac{\rho_v u^2 H}{2 D_e},$$

with a modified friction factor, five times than the smooth surface [6].

That is, for laminar flow, $f_v = 5(64/Re)$, the corresponding permeability $K_C = D_C^2/640$, for turbulent flow, $f_v = 5 \times 0.3164/Re^{0.25}$ and $K_C = D_C^2/0.8Re^{0.75}$.

In order to get the relationship of dried wall heat flux with the volume of the vapor channels from Eq. (8), some

additional approximations must be added. Generally, the vapor gravity can be neglected, and so, we can define

$$\left(\frac{\gamma}{k_{r\ell}}+\frac{1}{k_{rv}}\right)=C(S) \tag{15}$$

in here $\gamma=v_\ell/v_v$.

Integrating $C(S)$ from Eq. (10) as the saturation varies from 0 to 1 and denoting the integration value as C_1, or

$$C_1=\int_0^1\left(\frac{\gamma}{k_{r\ell}}+\frac{1}{k_{rv}}\right)^{-1}\mathrm{d}S =\int_0^1\left(\frac{1}{(1-S)^2}+\frac{\gamma}{S^3}\right)^{-1}\mathrm{d}S, \tag{16}$$

where $k_{r\ell}=S^3$ and $k_{rv}=(1-S)^2$ have been used in [12]. Then, by differentiating $\mathrm{d}J$ with $\mathrm{d}S$ and denoting the integration value of $\mathrm{d}J/\mathrm{d}S$ as C_2, we have

$$C_2=\int_0^1\frac{\mathrm{d}J}{\mathrm{d}S}\mathrm{d}S=\frac{-0.175}{\sqrt{5}}\int_0^1\frac{1}{S^2(S^{-1}-1)^{0.825}}\,\mathrm{d}S. \tag{17}$$

Integrating Eq. (8) with $\mathrm{d}x$ and introducing Eqs. (14) and (15), give

$$\frac{\sigma}{\sqrt{K/\phi}}C_2\frac{\mathrm{d}S}{\mathrm{d}S_P}\frac{\mathrm{d}S_P}{\mathrm{d}(x/H)}+\frac{v_vHq_{cr}}{Kh_{\ell v}}C_\ell-\rho_\ell gH=0, \tag{18}$$

where

$$\frac{\mathrm{d}S}{\mathrm{d}S_P}=\frac{\phi_PV_P}{\phi_PV_P+\phi_CV_C}. \tag{19}$$

Further integrating Eqs. (6a), (6b) over the boiling zone (i.e. porous layer height) subjected to the following boundary condition:

$$S_P=1,\quad \text{when } x/h=1, \tag{20}$$

$$\frac{\mathrm{d}S_P}{\mathrm{d}(x/H)}=0,\quad \text{when } x/H=1, \tag{21}$$

we obtain

$$q_{cr}=\frac{Kh_{\ell v}}{v_vH}C_\ell\left[\rho_\ell gH-\frac{\sigma}{\sqrt{K/\phi}}C_2\right]. \tag{22}$$

Eq. (22) provides the critical dry-out wall heat flux above which the vapor film will form on the heated surface for different channel population densities. Evidently, it is possible to maximize q_{cr} with respect to the density of vapor channels N_C for specific porous media ϕ_P, V_P and fluid.

4. Brief discussions

The experiment results show that the vapor channels opened to the heated surface improved the heat transfer rate furthermore as compared with for vapor channels not opened to the heated surface thoroughly [8]. The smaller the particle size and the heat flux are, the more the channel area ratio (CAR) should be opened. This trend seems to be consistent with the similar research on heat pipe wick experiments by Abou-Zyan and Plumb [5].

According to Stubos and Buchlin [6] model, the optimal channel area ratio will be 21%. 11% and 6% directed to 250, 110 and 65 μm, respectively, and the dry-out heat flux will be 10×10^5, 6×10^5 and 4×10^5 W/(m^2 K). Moreover, according to volume average model [9], the optimal channel area ratio will be 25%, 22% and 19% directed to 250, 110 and 65 μm, respectively, and the dry-out heat flux will be 2×10^5, 1×10^5 and 0.5×10^5 W/(m^2 K). Both of these two models show that the optimal channel area ratio decreased with particle size and wall hat flux. The contradiction may be caused by ignoring the smooth surface heat transfer in their models.

For the case of $H=3$ mm, $D_P=250$ μm, $D_C=1.5$ mm, $\phi=0.3$, the two-phase region will extent from 3 to 5.9 mm at the dry-out heat flux for R11 from Eq. (14). The dry-out heat flux of porous coating with vapor channels will be 7.5×10^5 W/m^2, which is about 10 times than the value calculated from isotropic porous coating.

Fig. 8 gives the relation of q_{cr} and the density of vapor channels N_C for the situations of R11 in [6]. ($A_v\times N_C=V_C$) the porous coatings were vented by boring holes in the surface. The fluid parameters were taken as: $\mu_\ell=2.825\times10^{-4}$ (Pa s), $\mu_v=1.2\times10^{-5}$ (Pa s), $\sigma=0.05886$ (N/m), $\rho_v=0.5977$ (kg/m^3), $\rho_\ell=958$ (kg/m^3), $h_{\ell v}=26.76\times10^5$ (J/kg). For the case of $H=8$ mm, $D_P=200$ μm, $D_C=1.5$ mm, $\phi=0.3$, the predicted

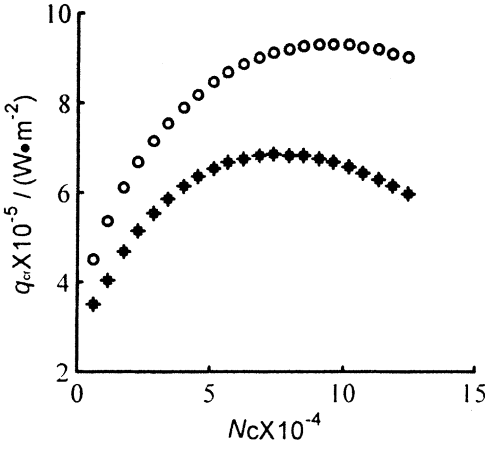

Fig. 8. Predicted dry-out heat flux as affected by the number of vapor channels: (○) $H=8$ mm, $D_P=300$ μm, $D_C=1.5$ mm, $\phi=0.4$; (∗) $H=8$ mm, $D_P=200$ μm, $D_C=1.5$ mm, $\phi=0.3$.

optimum area of the open channels is 12% and dry-out heat flux is 6.8×10^5 W/m^2 from the present model. The reported optimum area ratio of vapor channels is 25% and dry-out heat flux is 1.5×10^6 W/m^2 [6]. For the case $H = 8$ mm, $D_P = 300$ μm, $D_C = 1.5$ mm, $\phi = 0.4$, the calculated optimum area ratio of opened channels is 18% and dry-out heat flux is 9.3×10^5 W/m^2 from our present model. But the predicted optimum area ratio of the open channel is 32% and dry-out heat flux is 1.9×10^6 W/m^2, as reported in [6]. Since the dimension of the channels has an influence on the vapor flow resistance, the optimum area ratio of opened channels and dry-out heat flux will be changed accordingly. For channel width increased to 3.5 mm ($D_C = 3.5$ mm) in the second case, the predicted optimum area of opened channels is 18% and dry-out heat flux is 1.4×10^6 W/m^2 from the present model. But the optimum area ratio of opened channels is 24% and dry-out heat flux is 2.2×10^6 W/m^2 as reported in [6].

The simulated effects of the channel width 0.5 mm ($D_C = 1.5$ mm), $D_P = 250$ μm, $\phi = 0.3$, $H = 3$ mm are shown in Fig. 9 for R11. The predicted optimum area of vapor channels is 14% and dry-out wall heat flux is 7.4×10^5 W/m^2 from the model we suggested. The predicted value of the optimum area of vapor channels and dry-out heat flux are 25% and 3.3×10^6 W/m^2, respectively, by Stubo and Buchlin's model [6]. Our previous preliminary experiments demonstrate that the heat transfer on surface with opened channels is 15% [8]. The simulated effects of the case with channel width $W = 0.3$ mm, $D_P = 90$ μm, $H = 3$ mm are shown in Fig. 10 and the optimum area of channels is 10% and dry-out wall heat flux is 5.7×10^5 W/m^2.

The experimental dry-out heat fluxes are 3.5×10^5, 2×10^5 and 1×10^5 W/m^2 according to the Rainey and

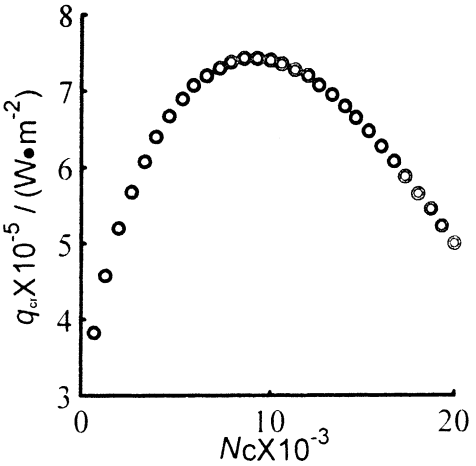

Fig. 9. Predicted dry-out heat flux as affected by the number of vapor channels; for $D_P = 250$ μm, $H = 3$ mm, $\phi = 0.3$, $W = 0.5$ mm.

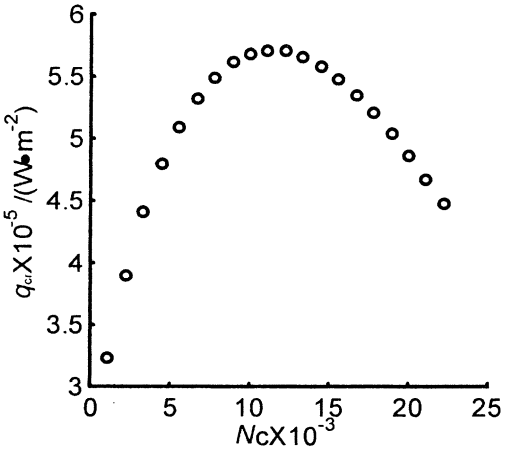

Fig. 10. Predicted dry-out heat flux as affected by the number of vapor channels; for $D_P = 90$ μm, $H = 3$ mm, $\phi = 0.3$, $W = 0.3$ mm.

You [10] criterion for pool boiling on plain and microporous pin finned surfaces. In short, further work would be necessary.

5. Conclusions

The heat transfer coefficient and $\dot{q}_{cr}$ of the porous surfaces with vapor channels were much higher than those on the smooth surface. Measurements of the pool boiling heat transfer on porous coated surfaces with vapor channels showed the existence of three regimes: liquid-flooding, bubbles in channel and bottom dry-out regions. In the bubble boiling region, bubbles escaped from the channels and heat transfer rate was enhanced by the ordered vapor–liquid flow. The results show that the size and density of the vapor channels affect the pool boiling heat transfer.

The dual porous equivalent model proposed here can reflect the mechanism of the process to some extent. The structural optimization of vapor channels, the effects of channel' dimension and density on the boiling heat transfer can be analyzed qualitatively. The optional channel density was obtained for specific porous surface, and the results are more reasonable than those in [6]. It is to be expected that this model can be used as a guide to conduct the experimental investigation. Further experimental and numerical work is needed to obtain the prediction of the optimum configuration of vapor channels more exact quantitatively.

Acknowledgements

The project is financially supported by the National Natural Science Foundation of China with Contract

number 59995550-3, and partly form the "985" Science Research Fund of Tsinghua University. We also sincerely thank Mr. Jin-Zhi HAO for his help.

References

[1] W.M. Rohsenow, J.P. Hartnett, E.N. Ganic, Handbook of Heat Transfer, McGraw-Hill, New York, 1987.
[2] S.A. Kovalev, S.L. Solovyev, G.A. Ovodkov, Liquid boiling on porous surfaces, Heat Transfer – Sov. Res. 19 (3) (1987) 109–120.
[3] R.A. Moss, A.J. Kelly, Neutron radiographic study of limiting heat pipe performance, Int. J. Heat Mass Transfer 13 (3) (1970) 491–502.
[4] S.P. Malyshenko, Features of heat transfer with boiling on surfaces with porous coating, Thermal Eng. 38 (2) (1991) 81–88.
[5] H.Z. Abou-Zyan, O.A. Plumb, Boiling on horizontal surfaces coated with porous metal wicks, HTD-Vol. 349, in: National Heat Transfer Conference, vol. 11, ASME, New York, 1997, pp. 90–95.
[6] A.K. Stubos, J.M. Buchlin, Enhanced cooling via boiling in porous layers: the effect of vapor channels, ASME J. Heat Transfer 121 (2) (1999) 205–209.
[7] M.P. Mughal, O.A. Plumb, An experimental study of boiling on a wicked surface, Int. J. Heat Mass Transfer 39 (1996) 771–777.
[8] W. Wu, J.-H. Du, B.-X. Wang, Boiling heat transfer on porous surfaces with vapor channels, J. Tsinghua Sci. Tech. (in English) (accepted).
[9] J.-H. Du, X.-J. Hu, B.-X. Wang, Dual porosity model on boiling heat transfer on porous surfaces with vapor channels, J. Tsinghua University (Natural Sci.) (in Chinese) 41 (10) (2001) 86–90.
[10] K.N. Rainey, S.M. You, Pool boiling heat transfer from plain and micoporous, square pin finned surfaces in saturated FC-72, HTD-Vol. 364-4, ASME, 1999, pp. 245–253.
[11] K.S. Udell, Heat transfer in porous media considering phase change and capillarity – the heat pipe effect, Int. J. Heat Mass Transfer 28 (2) (1985) 485–495.
[12] M. Kaviany, Principles of Heat Transfer in Porous Media, second ed., Springer, New York, 1996.